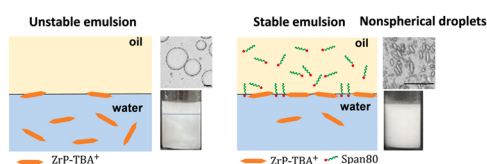


# A nanosheet-based combination emulsifier system for bulk-scale production of emulsions with elongated droplets and long-term stability

Nishat Anjum, Ya-Wen Chang, Siva A. Vanapalli<sup>\*</sup>

Department of Chemical Engineering, Texas Tech University, USA

## GRAPHICAL ABSTRACT



## ARTICLE INFO

### Keywords:

Emulsions  
Nano materials  
Phase inversion  
Anisotropic  
Stability

## ABSTRACT

In this study, we investigate the emulsion type, droplet morphology and emulsion stability that can be achieved using a novel combination emulsifier system which consists of water-soluble  $\alpha$ -zirconium phosphate tetrabutyl ammonium ( $\alpha$ -ZrP-TBA) nanosheets as the particulate emulsifier and Span 80 as the oil-soluble emulsifier, with the two emulsifiers present in distinct phases. We find that water-in-oil emulsions were formed for water volume fractions  $< 0.3$ , and oil-in-water (O/W) emulsions were formed for water volume fractions  $> 0.3$ . This phase inversion point was found to be the same irrespective of whether the emulsifier was only Span 80 or only nanosheet or their combination. Varying the concentrations of either surfactant or the nanosheet did not alter the phase inversion point. The emulsions with the greatest stability against creaming were formed using the combination emulsifier and were found to be the O/W type, that were stable for 3 months. Interestingly, we find that droplets in these stable emulsions were nonspherical, with the aspect ratio of droplets increasing with nanosheet and Span 80 concentration, suggesting a synergistic interaction between the two emulsifiers to create elongated droplets. We perform capillary neck thinning experiments to show that the combination emulsifier system offers unique interfacial properties that are different from either emulsifier alone, suggesting that interfacial jamming could occur to produce elongated droplets. Taken together, our results suggest a novel route to bulk-scale production of O/W emulsions that have long-term emulsion stability with unique droplet morphology.

## 1. Introduction

Emulsion is a thermodynamically unstable system in which the dispersed phase can be stabilized by conventional molecular surfactants or particulate emulsifiers [1,2]. Particle-stabilized emulsions, also known as Pickering emulsions [3], tend to provide enhanced emulsion

stability compared to surfactant-stabilized emulsions due to the irreversible adsorption of particles at the interface. The high energy of particle adsorption to the interface relative to thermal energy leads to the formation of densely packed particle layers providing stability for the emulsion [2,4]. Despite the distinct advantages of particulate emulsifiers for emulsion stabilization, limitations can exist in terms of

<sup>\*</sup> Corresponding author.

E-mail address: [Siva.Vanapalli@ttu.edu](mailto:Siva.Vanapalli@ttu.edu) (S.A. Vanapalli).

<https://doi.org/10.1016/j.colsurfa.2022.128403>

Received 16 October 2021; Received in revised form 29 December 2021; Accepted 21 January 2022

Available online 25 January 2022

0927-7757/© 2022 Elsevier B.V. All rights reserved.

the wettability of the particles at the interface or being prone to aggregation. These limitations are addressed by coating/grafting treatment [5,6] to modify the surface properties of particles. It is also common practice to modify wettability through adsorption of surfactants [7–11], where the ratio of surfactants and particles needs to be tuned in order to avoid flocculation. In fact, many commercial emulsions such as drilling fluids [12], paints [13], food [14] contain both surfactants and particles.

Two possibilities exist for using a combination of surfactants and particulate emulsifiers depending on the phase in which they are dispersed. In the first case, surfactants and particles are mixed into the same phase (typically aqueous phase), and several studies have investigated emulsion stability with such mixtures [7–10,15–21]. Because both the surfactant and the particles were dispersed in the same phase, it is expected that the surfactants can adsorb on the particles to tailor the wettability even before emulsification. In the second case, the surfactant and particles are present in different phases, with typically the surfactant being in the oil phase and the particles being in the water phase [22–29] (for example, see Table 1). Here, the interaction between both emulsifiers does not occur before emulsification since they are in different phases. This second case has been less studied in the context of emulsion stability and is the focus of our investigation.

With respect to particulate emulsifiers, their size, shape, and surface chemistry become important factors for determining the stability of emulsions against coalescence [30,31]. Nonspherical particles with a high aspect ratio such as disk-like laponite clay [32–34], rod-like chitin nanocrystals [35], single-walled carbon nanotubes (SWNTs) [36,37], and graphene oxide (GO) nanosheets [38–41] have been used as emulsion stabilizers. The atomically thin two-dimensional (2D) materials are more efficient than spheres due to strong adsorption at the interface [31]. Additionally, nanosheets provide more surface area per unit mass compared to equivalent spheres, making 2D nanomaterials attractive for emulsion stabilization [42].

Among the available nanomaterials, layered nanomaterials are unique because single nanosheets can be obtained by chemical exfoliation due to electrostatic repulsion between the layers. Examples include inorganic materials such as clay,  $\alpha$ -zirconium phosphates ( $\alpha$ -ZrP), niobates, titanates, or organic materials, such as graphite [43]. Among these, nanosheets made from  $\alpha$ -ZrP have several advantages. First, the aspect ratio of the nanosheet can be altered easily by varying phosphoric acid concentration, reaction time, and reaction temperature, resulting in layered  $\alpha$ -ZrP crystals of different lateral sizes and polydispersity [44, 45]. The thickness of the nanosheet can also be modified by different adsorbed counterion layers. Second, due to the counter cations present on the particle surface such as tetrabutyl ammonium (TBA) ions (that comes from the tetrabutyl ammonium hydroxide used in the exfoliation process), the  $\alpha$ -ZrP-TBA nanosheet dispersion is less prone to aggregation at neutral pH conditions, unlike clay, graphene, or graphene oxide (GO). Finally, unlike graphene nanosheet, which is difficult to obtain due to complex chemical processes [46,47], the synthesis of  $\alpha$ -ZrP nanosheet is a simple process involving easy synthesis along with

complete exfoliation.

There has been limited work on using  $\alpha$ -ZrP nanosheets for emulsion stabilization. Meija et al. [48] investigated the stability of emulsions with amphiphilic  $\alpha$ -ZrP-TBA nanosheets, which were chemically modified with octadecyl isocyanate (ODI). It was found that compared to non-modified nanosheet ( $\alpha$ -ZrP-TBA), modified nanosheet ( $\alpha$ -ZrP-ODI) was a better stabilizer forming stable oil-in-water (O/W) emulsions with spherical droplets that lasted for a month. However, they only investigated the stability of O/W emulsion within a small range of volume fraction of oil ( $0.082 < \phi_o < 0.12$ ) as a function of nanosheet concentration. Guevara et al. [49] stabilized the Pickering foam with the high aspect ratio nanosheet ( $\alpha$ -ZrP-PA) where  $\alpha$ -ZrP crystals were exfoliated with propylamine ( $C_3H_7NH_2$ , PA). The impact of the aspect ratio of nanosheets, concentration, and hydrophobicity on the stability of air-water interfaces was studied. They discovered that high aspect ratio nano-sheets with high and intermediate hydrophobicity were the most effective for achieving stable foam, lasting for 36 days, and formed nonspherical bubbles.

A survey of literature reveals that although emulsion studies with nanosheets from  $\alpha$ -ZrP crystals have been conducted, none were conducted using a combination of these nanosheets and surfactants. Likewise, as shown in Table 1, although several studies have been conducted with 2D nanomaterials and surfactants, but no studies exist using the  $\alpha$ -ZrP-TBA nanosheets and a lipophilic surfactant. Moreover, some of these studies did not systematically investigate emulsion type that can be achieved by varying the volume fraction over a wide range.

Another emerging research frontier involving particulate emulsifiers is the ability to create emulsions containing non-spherical droplets since nanoparticles and surfactants can produce jammed interfaces. One class of methods uses nanoparticle surfactants in combination with external fields to produce nonspherical droplets, as pioneered by Russell and co-workers [50–52]. In this case, the electric or magnetic fields deform the interface promoting interfacial adsorption and jamming of the nanoparticle surfactants, thereby preventing relaxation to spherical shape. The other class of methods uses crystallizable oils along with geometric confinement and temperature shift to produce rod-shaped emulsion droplets [53–55]. Here, the elasticity of the solidifying droplets overcomes the Laplace pressure to retain the elongated shape, which vanishes when the droplet is liquified. In both classes, the throughput is limited since droplets are made one-by-one. Importantly, there is a need to evaluate the long-term stability of the emulsions containing non-spherical droplets with respect to phase separation, and such studies are lacking.

In this study, we employ the combination emulsifier approach using nanosheets derived from  $\alpha$ -ZrP crystals as water-soluble particulate emulsifiers and Span 80 as the oil-soluble surfactant and study the type of emulsions that can be formed and their stability. Unlike, the common strategy of mixing nanoparticles and surfactants in bulk in the same phase, here the two emulsifiers do not come into contact except at the interface when the droplets are formed. Initially, we characterize the interfacial activity of nanosheets in the presence of Span 80. We then

**Table 1**

Studies that investigated emulsion stability with particulate emulsifiers (2D Nanomaterials) in the aqueous phase and an oil-soluble surfactant in the dispersed phase.

Study	Oil phase	Oil-soluble surfactant	2D nanomaterial	Water or oil volume fraction, $\phi$
Lagaly et al. [24]	paraffin oil	glycerol monostearate, deca(ethylene glycol) hexadecyl ether, alkyl polyglucoside lecithin	bentonites, montmorillonite, hectorites	$0.1 < \phi \leq 0.5$
Whitby et al. [25]	dodecane	octadecyl amine octadecanoic acid	laponite	0.5
Wang et al. [27]	paraffin oil	Span 80	laponite, layered double hydroxide	0.5
Zhang et al. [28]	paraffin oil	Span 80	laponite	0.5
Nallamilli and Basavaraj [29]	n-decane	Span 80	kaolinite	$0.1 \leq \phi \leq 0.9$
This work	mineral oil	Span 80	$\alpha$ -ZrP-TBA nanosheets	$0.1 \leq \phi \leq 0.9$

systematically vary the surfactant and nanosheet concentrations, and investigate the critical volume fraction at which phase inversion occurs. We evaluate the stability of these emulsions against creaming/sedimentation and find that the combination emulsifier system can stabilize O/W emulsions upto 3 months. Intriguingly, the droplet morphology in these stable emulsions was found to be elongated with an aspect ratio that increases with increasing concentration of nanosheet and Span 80. Finally, we conduct capillary breakup experiments and find supporting evidence that the nanosheet and Span 80 synergistically interact to create a solid-like interface that promotes the formation of elongated droplets. Taken together, our study highlights a novel route for the bulk-scale production of stable emulsions with unique droplet morphology.

## 2. Materials and methods

### 2.1. Materials

Zirconyl chloride octahydrate ( $\text{ZrOCl}_2 \cdot 8\text{H}_2\text{O}$ , 98+%, ACROS Organics, NJ, USA), Phosphoric Acid ( $\text{H}_3\text{PO}_4$ , 85 wt%, Fisher Scientific, NH, USA), Tetrabutylammonium hydroxide (TBAOH, 40 wt% (1.5 M) solution in water, ACROS Organics, NJ, USA), Span 80 (Sigma-Aldrich,

MO, USA), Mineral Oil, Light (Fisher Scientific, NH, USA), Nile red (Fisher Scientific, NH, USA) and Fluorescein (Fisher Scientific, NH, USA) were used as received. Deionized water (DI) was obtained from Milli-Q (Millipore Sigma, MA, USA) system.

### 2.2. Synthesis and characterization of $\alpha$ -ZrP-TBA nanosheets

Crystalline  $\alpha$ -zirconium phosphate ( $\alpha$ -ZrP) particles were synthesized using hydrothermal method [44,45]. 6 g of Zirconyl chloride octahydrate was mixed with 12 mL of water and added dropwise in 48 mL of 15 M phosphoric acid solution under vigorous stirring for 24 h to yield a final concentration of 12 M phosphoric acid. The resulting homogenous solutions were poured into a 100 mL PTFE container and put in an autoclave for 24 h at 200 °C to make the  $\alpha$ -ZrP particles.

The  $\alpha$ -ZrP particles were washed with DI water three times and collected by centrifugation. The crystals were dried in the oven at 60 °C overnight and ground with mortar and pestle into fine powder. Fig. 1a shows the scanning electron micrographs (obtained using the S-4300 E/N (FESEM), Hitachi, Tokyo, Japan operated at 5.0 kV) of the pristine layered  $\alpha$ -ZrP crystals.

The nanosheets were prepared through intercalation and exfoliation

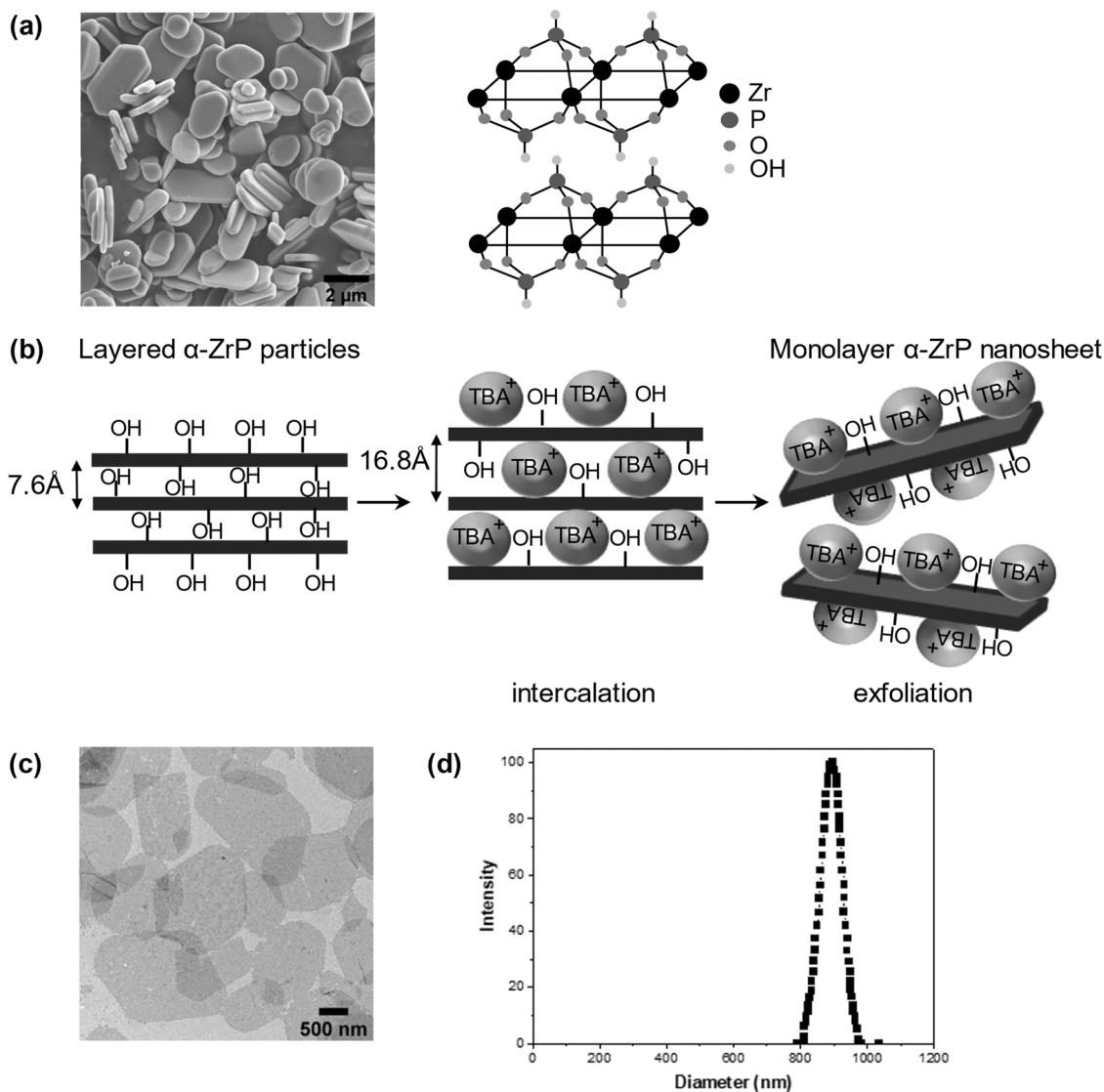


**Fig. 1.** Synthesis and characterization of nanosheets exfoliated from  $\alpha$ -ZrP particles using TBAOH. (a) Scanning electron microscopy (SEM) images of pristine  $\alpha$ -ZrP particles. The crystal structure is shown on the right side. (b) Schematic showing the intercalation and exfoliation process of nanosheets from the  $\alpha$ -ZrP layered particles. (c) Transmission electron microscopy (TEM) micrographs of nanosheets after exfoliation. (d) The size distribution of nanosheets.

of layered  $\alpha$ -ZrP crystals (Fig. 1b). A known amount of particle powder was combined with TBAOH at an equal molar ratio. For instance, 2 g of ZrP powder was dispersed in 24.67 mL of DI water and charged with 4.33 mL of TBAOH. The mixture was then vortexed extensively at 10,000 rpm and subjected to sonication in an ice bath for 30 min. The suspension was equilibrated for 48 h at room temperature. The exfoliated nanosheets were collected through centrifugation and re-dilution with water three times to remove the sedimented non-exfoliated particles. The  $\alpha$ -ZrP-TBA nanosheet concentration was determined by drying a known amount of sample.

Transmission Electron Microscope (H-8100 Scanning/Transmission Electron Microscope (STEM) Hitachi, Tokyo, Japan) operated at 200kV was used to image the  $\alpha$ -ZrP-TBA nanosheets. A drop of the nanosheet suspension was dried on a carbon-coated copper grid at room temperature. From the TEM micrographs, the hexagonal shape of nanosheets was confirmed after the exfoliation of pristine ZrP crystals (Fig. 1c).

The size distribution of nanosheets was obtained using dynamic light scattering analysis (NanoBrook Omni, Brookhaven Instruments Corporation, NY, USA), shown in Fig. 1d. The zeta potential of non-exfoliated  $\alpha$ -ZrP particles and the  $\alpha$ -ZrP-TBA nanosheets was also determined using phase analysis light scattering. The zeta potential of non-exfoliated  $\alpha$ -ZrP particles was  $-56.69 \pm 2.12$  mV, whereas that of the  $\alpha$ -ZrP-TBA nanosheets was  $-26.72 \pm 3.06$  mV. The zeta potential of the nanosheets is lowered due to the presence of positively charged TBA<sup>+</sup> ions.

### 2.3. Preparation and characterization of emulsions

Different concentrations of  $\alpha$ -ZrP-TBA nanosheets were suspended in DI water and mixed with mineral oil containing Span 80 surfactant at different volume fractions of water by vortex mixing at 2000 rpm for 2 min. The emulsion type was determined by visual phase separation and fluorescence micrographs. The emulsion was deemed as oil-in-water (O/W) if there was a clear water phase at the bottom with a creamed emulsion layer. The emulsion was deemed water-in-oil (W/O) if there was a clear oil phase at the top and a sedimented emulsion layer at the bottom [56]. Photographs of vials containing emulsion were taken with iPhone 6splus after 24 h and 3 months. The height of the separated emulsion layers was determined using ImageJ (version 1.5) software as a measure of the emulsion stability.

Fluorescence imaging was used to identify the emulsion type when there was no visibly clear creaming/sedimentation. The oil-soluble (0.02 wt%) Nile red and the water-soluble (0.01 wt%) fluorescein was used to determine whether it was an O/W emulsion or a W/O emulsion after observation of droplet images under the microscope. (Nikon Eclipse Ts2, Nikon Instrument Inc. NY, USA).

### 2.4. Interfacial tension using the pendant drop

The interfacial tension (IFT) was measured by a custom-built pendant drop apparatus [57]. A 27-gauge needle connected to a 1 mL syringe on a syringe pump (Chemyx Inc Fusion 200, Fisher Scientific, NH, USA) was used to form a pendant drop. The water containing different concentrations of  $\alpha$ -ZrP-TBA nanosheets was loaded into syringes. The X-Y-Z translational control knob was used to insert the needle into a 1 cm x 1 cm plastic cuvette containing mineral oil with Span 80. Illumination was achieved using a lamp (QTH10, Thorlabs, NJ, USA) along with a diffuser. A series of time sequence images were captured for 1800 s at a frame rate of 6 images per minute using the camera (DMK 23UP1300, The Imaging Source, NC, USA) with the software IC Capture (version 2.3). All the experiments were performed at  $22 \pm 2$  °C. The interfacial tension was then calculated in Image J (version 1.5) using the drop analysis plug-in by fitting the contour of the drop with the Young Laplace equation.

### 2.5. Neck thinning dynamics during drop breakup in a microcapillary device

The co-flow geometry was built in a glass-based capillary device [58]. The inner capillary tube was cylindrical with a circular cross-section—the tapered tip with an inner diameter of  $d_{\text{tip}} = 60$   $\mu\text{m}$  and an outer diameter of 95  $\mu\text{m}$ . The outer diameter of the untapered portion of the inner capillary was  $D = 1$  mm, which matched the inner dimensions ( $1.00 \times 1.00$  mm<sup>2</sup>) of the hollow square glass capillary, facilitating co-axial alignment. The glass capillaries were purchased from VitroCom, NJ, USA.

The  $\alpha$ -ZrP nanosheet exfoliated with TBAOH ( $\alpha$ -ZrP-TBA nanosheet) was dispersed in de-ionized water at 5 wt% concentration and its viscosity was measured to be  $\approx 11$  mPa.s. The oil-soluble surfactant sorbitan monooleate (Span 80) was dissolved at 1 wt% in mineral oil. The viscosity of mineral oil was measured to be 50 mPa.s. The viscosities were measured using TA Discovery HR-2 rheometer (TA instruments, DE, USA) with cone and plate geometry (25 mm plate diameter, 1° cone, gap of 0.05 mm) at 25° C.

The dispersed phase (mineral oil or mineral oil containing 1 wt% Span 80) was injected through the cylindrical capillary into the square capillary containing the continuous phase (de-ionized water or 5 wt% nanosheet dispersion). The hydrophilic tip was used to produce an oil-in-water (O/W) emulsion. The flow rates of the continuous phase ( $Q_{\text{out}} = 80$  mL/h) and the dispersed phase ( $Q_{\text{in}} = 0.5$  mL/h) were varied using syringe pumps (Fusion 200 and Nexus 3000 Chemyx Inc, TX, USA). The droplet formation was recorded at the capillary tip using a high-speed camera (Phantom VEO-E 310 L, Vision Research, NJ, USA) attached to an inverted microscope (ECLIPSE Ts2, Nikon Instrument Inc. NY, USA).

The images in the dripping regime were acquired at 20,000 fps with 20X magnification to examine the thinning dynamics of the neck during dripping. Images of size  $512 \times 256$  pixels were acquired with each pixel corresponding to 1.22  $\mu\text{m}$ . A custom-written image processing code in MATLAB (R2021a, Mathworks, USA) was used to process the images to extract the neck thinning information. First, the region of image analysis was selected based on where the neck thinning was observed. Next, a background image of the viewing area was acquired before the pinch-off experiment. The experimental frames and background image were inverted prior to background subtraction since neck borders are dark pixels. The subtracted images were then transformed to a binary image with a noise-removal threshold. The borders of the thinning neck were detected based on the transition from black to white pixel. The neck diameter was determined by the minimum value between the two edges at the time that images were taken. Finally, a Savitzky-Golay filter was used to smooth the data of neck thinning. The filter fits a polynomial to a window of data as the window passes over the data. Here, a window size of 11 data points was used to fit a first-order polynomial at each window.

## 3. Results

### 3.1. Interfacial activity of ZrP-TBA nanosheets and Span 80

To assess the ability of  $\alpha$ -ZrP-TBA nanosheets to make emulsions, we determined their interfacial activity. Even though the nanosheet itself is hydrophilic due to their water-soluble nature, the tetrabutyl groups on the nanosheet surface can provide some lipophilic character, making the  $\alpha$ -ZrP-TBA nanosheets potentially amphiphilic. The interfacial activity of the  $\alpha$ -ZrP-TBA nanosheets was determined by measuring the equilibrium interfacial tension (IFT) at several different concentrations of  $\alpha$ -ZrP-TBA nanosheets in the range of 0–5 wt%. As shown in Fig. 2a, in the absence of nanosheets the equilibrium IFT was  $57.43 \pm 0.89$  mN/m. With increasing nanosheet concentration, the equilibrium IFT decreased to as low as  $30.82 \pm 2.04$  mN/m at 5 wt% concentration; thus, reducing the IFT to  $\approx 47\%$  of its original value.

The amphiphilic nature of  $\alpha$ -ZrP-TBA nanosheets and its adsorption to

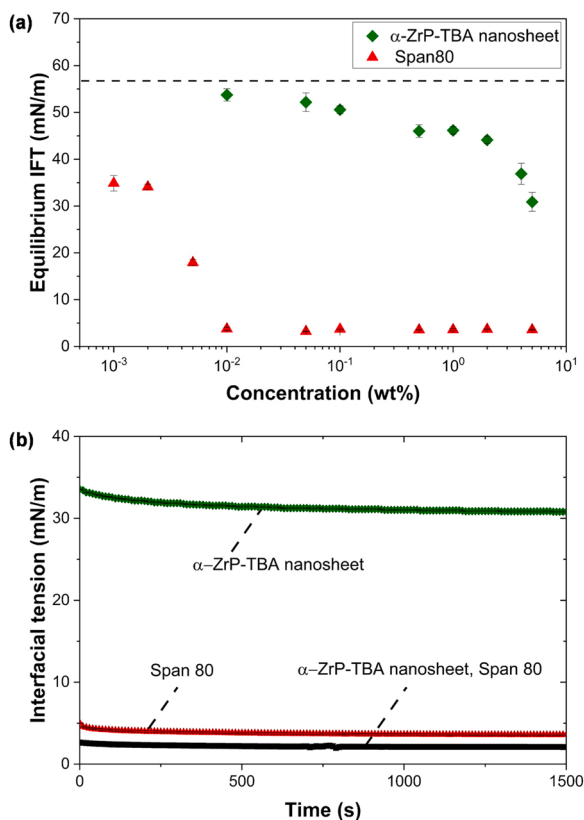


**Fig. 2.** Effect of  $\alpha$ -ZrP-TBA nanosheet and Span 80 concentration on interfacial tension in the mineral oil and water system. (a) Equilibrium interfacial tension due to the presence of only  $\alpha$ -ZrPTBA nanosheets or only Span 80. (b) Interfacial tension as a function of time due to 5 wt%  $\alpha$ -ZrPTBA nanosheets or 1 wt% Span 80 or their combination at these respective concentrations.

the oil-water interface could be due to the surface cations TBA<sup>+</sup> which are hydrophobic nature. The explanation of particle attraction to the interface is supported by the measurement of ion hydrophobicity in the literature: Octanol-water partition coefficient of TBA<sup>+</sup> is 0.7726 [59]. The TBA<sup>+</sup> ion concentration affected the interfacial tension as well. A decrease in surface and interfacial tension with increasing concentration of tetrabutylammonium halides has been reported [60] similar to our result.

In Fig. 2a, we show the equilibrium IFT data in the presence of Span 80 alone. The interfacial activity of the surfactant was determined by measuring the equilibrium interfacial tension (IFT) at several different concentrations of Span 80 in the range of 0–5 wt%. After adding Span 80, the interfacial tension decreased with increasing concentration until the critical micelle concentration (CMC ~ 0.01 wt%) and then reached a plateau value of  $3.58 \pm 0.29$  mN/m. Thus, compared to  $\alpha$ -ZrP-TBA nanosheets which lowered the interfacial tension of the bare interface by about  $\approx 2$  times, Span 80 lowered the interfacial tension by about  $\approx 16$  times suggesting that Span 80 has higher interfacial activity and therefore a better emulsifier.

Next, we investigated changes in IFT over time in the combination system of  $\alpha$ -ZrP-TBA nanosheets and Span 80 and compared the data to the individual systems. As shown in Fig. 2b, we find that in all three cases, equilibrium IFT is reached in less than 10 s. Interestingly, we find that the IFT data for the combination system is closer to the IFT data for the Span 80 system indicating that the interfacial activity in the combination case is dominated by Span 80. Nevertheless, including  $\alpha$ -ZrP-TBA nanosheets along with Span 80 led to a small but significant reduction in IFT of  $\approx 40\%$  compared to the Span 80 alone system.

It appears that in the combination system, the Span 80 molecules present in the oil phase are able to occupy the interface and are more

effective at reducing the interfacial tension. The molecular.

size of Span 80 is  $\approx 1.1$  nm [61], and that of  $\alpha$ -ZrP-TBA nanosheets is  $\approx 1000$  nm. The calculated Stokes-Einstein diffusivities for these two emulsifiers in their respective solvents are  $\approx 3.96 \times 10^{-12}$  m<sup>2</sup>/s and  $2.18 \times 10^{-13}$  m<sup>2</sup>/s suggesting that Span 80 is able to diffuse  $\approx 18$  times faster than the nanosheets and dominate the interfacial activity of the combination system.

### 3.2. Emulsion type and stability of $\alpha$ -ZrP-TBA-nanosheet-stabilized emulsions

The IFT studies showed that  $\alpha$ -ZrP-TBA nanosheets can lower the interfacial tension of the bare oil-water interface by about half. So, we tested the type of emulsions that can be made using 5 wt% nanosheet dispersion and assessed the emulsion stability. Fig. 3a shows microscopy images of droplets from emulsions that were made and visualized right after their production. The emulsions were made with volume fraction of water  $\phi_w$  varying from 0.1 to 0.9. We find that for  $\phi_w < 0.3$ , the emulsions are W/O type since the water-soluble fluorescent dye was found in the droplets. Likewise, we observe that for  $\phi_w > 0.3$  the emulsions are O/W type. Thus, the catastrophic phase inversion occurred at a critical volume fraction of  $\phi_{cw} = 0.3$ . Additionally, from the brightfield images we found that the droplets from the W/O emulsion were partially wetting the glass slide indicating poor emulsion stability, while the O/W emulsion droplets were non-wetting due to the retention of their spherical shape.

Next, we evaluated the stability of the emulsions by examining their phase separation at 24 h after preparation, as shown in Fig. 3b. We found that the W/O emulsions were more susceptible to phase separation than the O/W emulsions as evident by the clear oil layer in emulsions with  $\phi_w < 0.3$ . This suggests that the nanosheet as a particulate emulsifier is better at stabilizing O/W emulsions than W/O emulsions, although the O/W emulsions do not retain 24-h stability since some degree of phase separation is observed in all the O/W emulsions.

Interestingly in Fig. 3b, we find that beyond the phase inversion point in the O/W emulsions, the height of the phase separated layer increases with an increase in water fraction. Thus, the creamed layer height decreases with the increase in water fraction (Fig. 3c) in O/W emulsions suggesting that droplet-droplet interactions or crowding inhibit creaming. In addition to the experiments in Fig. 3b, where 5 wt% nanosheet was used, we also tested creaming in the O/W emulsions (with  $\phi_w = 0.8, 0.9$  i.e. oil fraction of 20% and 10% respectively) by increasing the nanosheet concentration from 0 to 5 wt% (Fig. 3d). We found that irrespective of the nanosheet concentration, the creamed layer height was the same indicating that the concentration of nanosheet does not strongly influence the creamed layer thickness but is more dominated by the concentration of oil droplets in the O/W emulsion.

### 3.3. Emulsion type and stability using the combination emulsifier system

We tested the effect of the combination emulsifier system with the nanosheets in the aqueous phase and 1 wt% Span 80 in the oil phase. As shown in Fig. 4a, b for all the tested nanosheet concentrations, the phase inversion occurs at a critical water fraction of  $\phi_{cw} = 0.3$ . Thus, similar to the nanosheet-alone system, in the combination emulsifier system as well, we find that W/O emulsions are formed at  $\phi_w < 0.3$  and O/W emulsions are formed at  $\phi_w > 0.3$ . Another important observation is that in the presence of Span 80 alone, stable W/O emulsions are formed initially since the O/W emulsions cream, although 24-h emulsion stability is not conferred. Hence, neither surfactant nor exfoliated nanosheets alone do not offer 24-h stability against coalescence.

When we explored the effect of nanosheet concentration, from Fig. 4a,b it is evident that for  $\phi_w < 0.3$ , the W/O emulsions are stable at all the tested nanosheet concentrations. However, for  $\phi_w > 0.3$ , the stability depends on the nanosheet concentration, with O/W emulsions being more stable at higher nanosheet concentration. To quantitate this

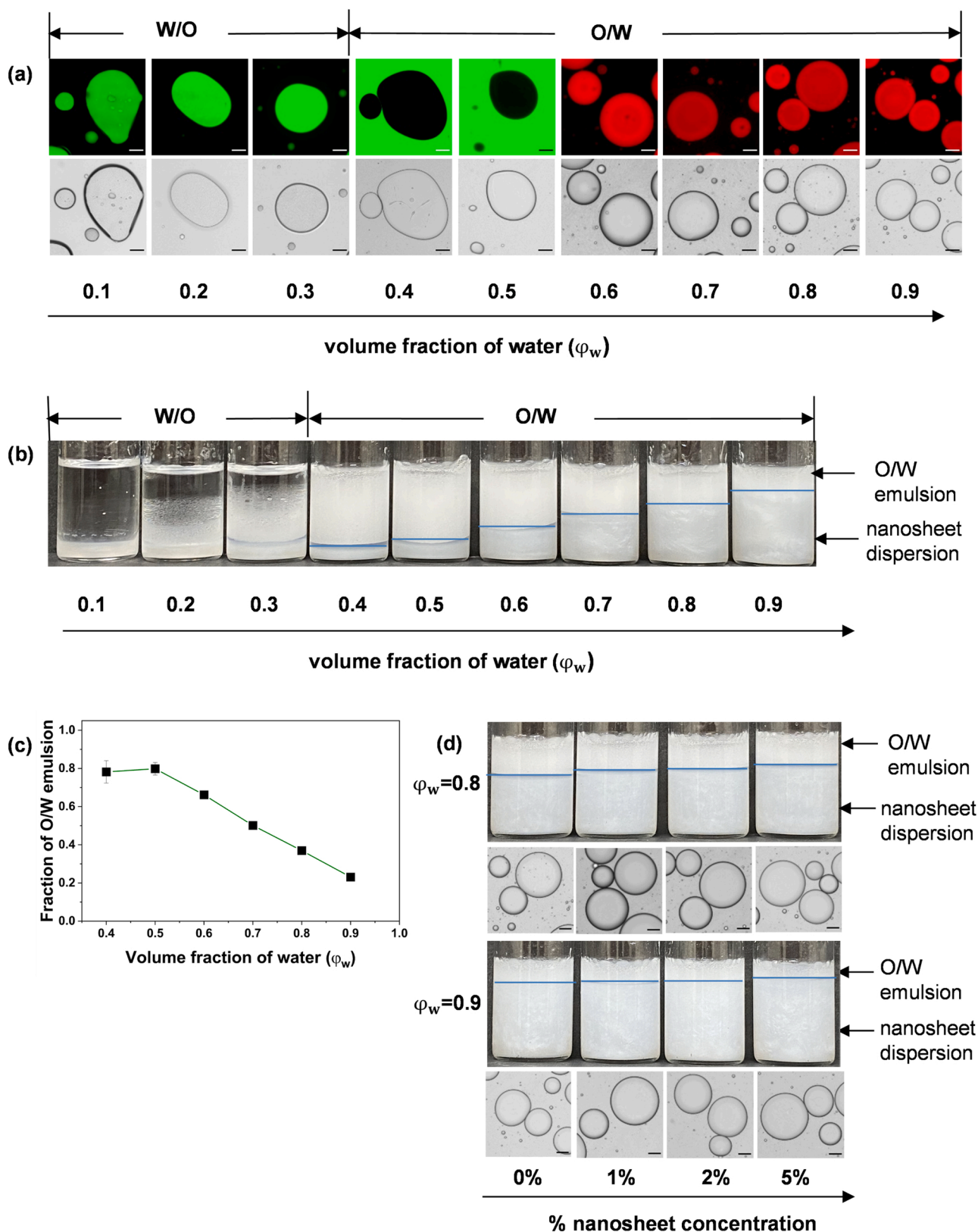


**Fig. 3.** Effect of  $\alpha$ -ZrP-TBA nanosheet alone on emulsion stability and droplet morphology. (a) Optical micrographs of emulsion stabilized by 5 wt%  $\alpha$ -ZrP-TBA nanosheet alone under fluorescence and bright field immediately after preparation. (b) Emulsion stabilized by  $\alpha$ -ZrP-TBA nanosheet alone at 24 h after preparation. (c) The fraction of O/W emulsion as a function of volume fraction of water ( $\phi_w$ ) at 24 h after preparation. The volume fraction of water is displayed below the figure. (d) Depletion experiment for  $\alpha$ -ZrP-TBA nanosheet system. The volume fraction of water ( $\phi_w$ ) = 0.8 and 0.9 are selected for this experiment (included in the left side of figure). The volume fraction ( $\phi_w$ =0.8, 0.9) of nanosheet is increased from 1% to 5% at fixed total volume of solution (= 2 mL), indicated below the figure. The pictures of vials and optical images were taken after preparation at 24 h and immediately, respectively. The line indicates the height of  $\alpha$ -ZrP-TBA nanosheet dispersion. The scale bar is 80  $\mu$ m.

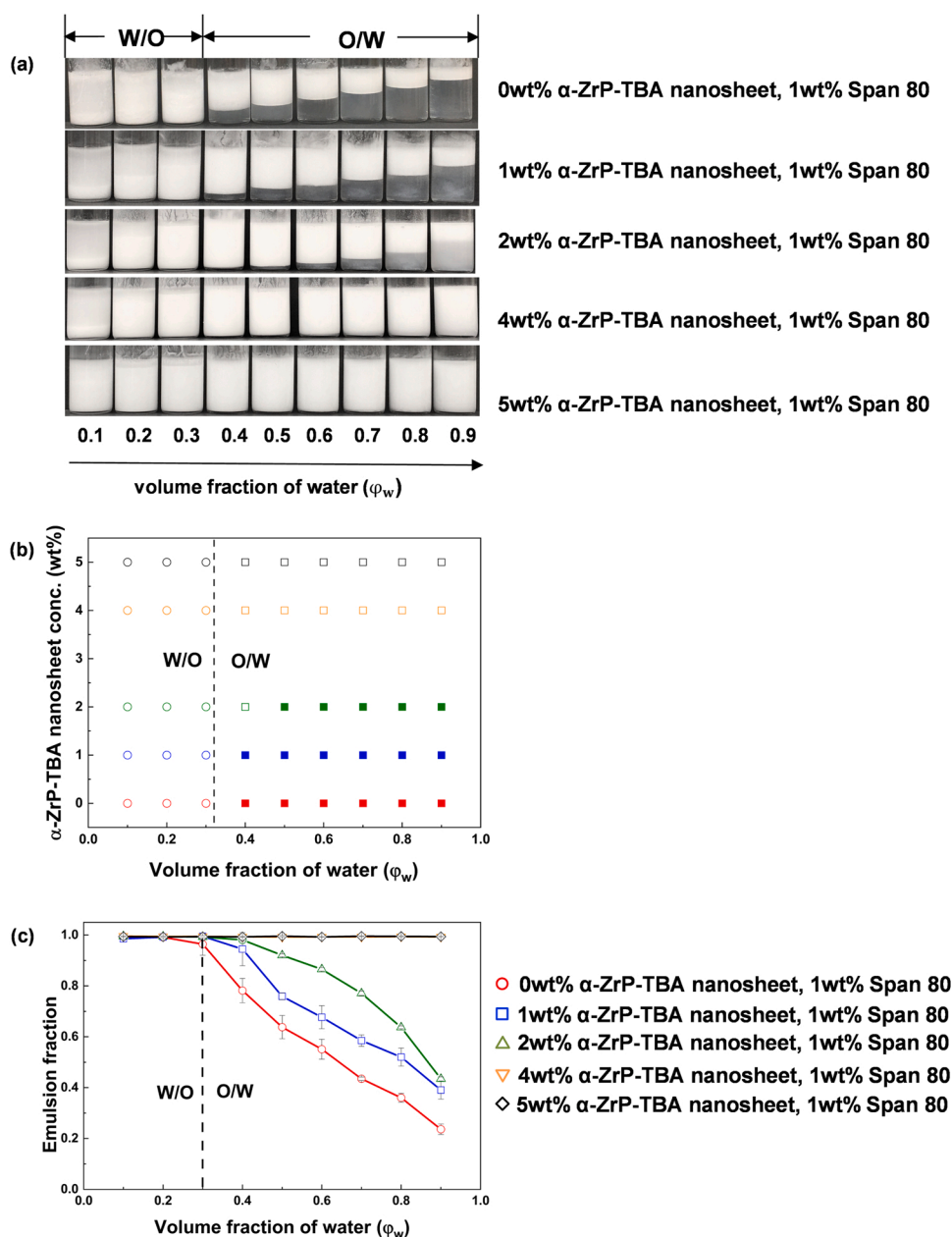


**Fig. 4.** Type and stability of the emulsion when using the combination system of  $\alpha$ -ZrP-TBA nanosheet and Span 80. (a) Images showing the phase separation of emulsions stabilized by surfactant and particulate emulsifier for different volume fraction of water at 24 h after preparation. (b) Emulsion state diagram indicating the type of emulsions formed and their stability at 24 h. The open and filled symbols correspond to stable (no separation at 24 h) and unstable (separation at 24 h) emulsion, whereas circle and square correspond to W/O emulsion and O/W emulsion, respectively. (c) Emulsion fraction as a function of volume fraction of water at 24 h after preparation. Lines are a guide to the eye.

stability, the emulsion fraction was plotted as a function of the volume fraction of water for different  $\alpha$ -ZrP-TBA concentrations after 24 h of preparation, as shown in Fig. 4c. The emulsion fraction was calculated as the ratio of the height of the emulsion layer (from either creaming or sedimentation) to the total height of the solution. A large value of emulsion fraction indicates high emulsion stability. The 24-h stability of W/O emulsion is independent of the volume fraction of water and nanosheet concentration. In contrast, the O/W emulsion stability decreases with the increase in volume fraction of water. However, as the nanosheet concentration increases, the emulsion fraction increases, suggesting ZrP-TBA nanosheets at high concentration enhanced the stability of O/W emulsion.

In addition to the 24-h stability, we also evaluated long-term emulsion stability when using the combination emulsifiers by monitoring the creaming/sedimentation over a period of 3 months (Fig. 5a). Even though the W/O emulsions were stable for 24 h, they lacked long-term stability despite high particle loading. Similar to the W/O emulsions, the O/W emulsions also lacked long-term stability except when the

combination emulsifier contained 5 wt%  $\alpha$ -ZrP-TBA. The creaming kinetics were monitored at different nanosheet concentrations at a fixed volume fraction of water ( $\phi_w = 0.7$ ) (Fig. 5b). The fraction of emulsion increases with an increase in nanosheet concentration. Emulsion seems stable when using 5 wt%  $\alpha$ -ZrP-TBA for at least 1 month with a slight creaming after this period. We also compared the long-term stability (up to 1 month) of emulsions ( $\phi_w = 0.9$ ) with Span 80 concentrations of 0.1, 0.5 and 1 wt%, while keeping the nanosheet concentration at 5 wt%. We found that the creaming stability improved with increasing Span 80 concentration. Thus, the synergistic effect between the lipophilic nonionic surfactant and the hydrophilic ZrP-TBA nanosheet is required for the long-term stability of O/W emulsions.

We also evaluated whether the enhanced viscosity of nanosheet dispersion at 5 wt% could contribute to the long-term stability. Compared to low nanosheet concentration such as 2 wt%  $\alpha$ -ZrP-TBA, whose viscosity is 4 mPa.s, the viscosity of the highest nanosheet concentration of 5 wt% is  $\approx 11$  mPa.s, which is almost 2.5x higher. If it was purely a viscosity effect, this enhanced viscosity should lead to a

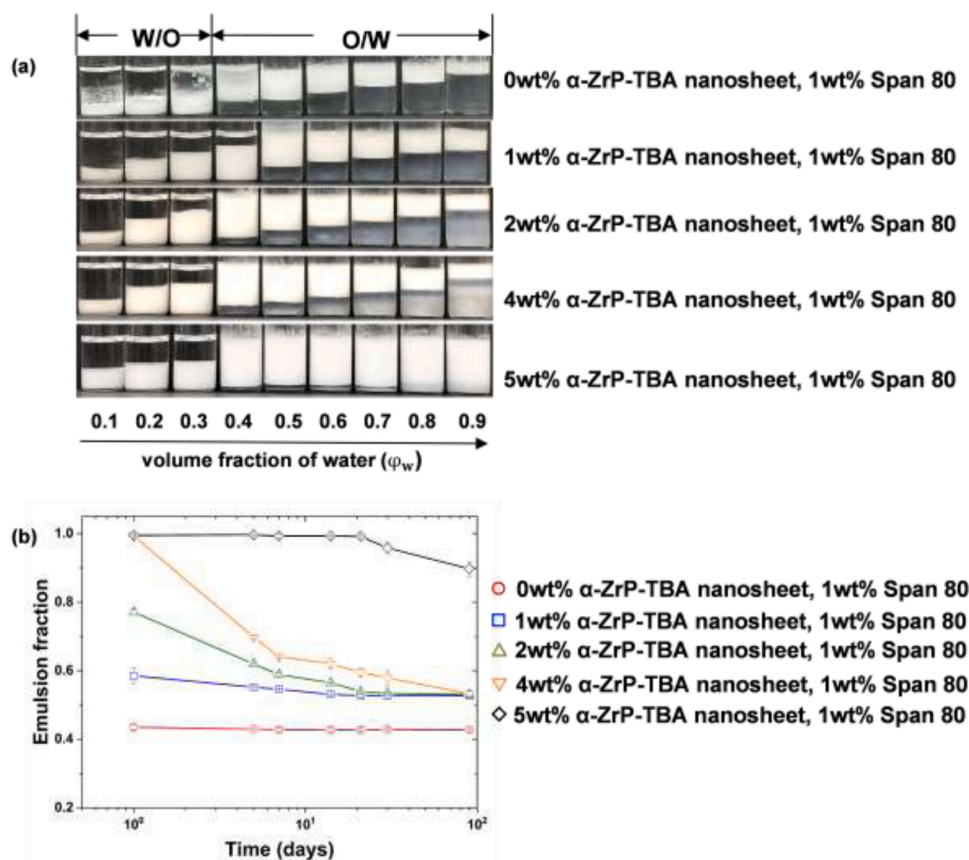


**Fig. 5.** Long-term (at 3 months) stability of the emulsion when using the combination emulsifier system of  $\alpha$ -ZrP-TBA nanosheet and Span 80. (a) Images showing phase separation for different volume fraction of water at 3 months after preparation. (b) Creaming kinetics for a fixed volume water fraction of  $\phi_w = 0.7$ , evaluated upto 3 months after preparation. Lines are a guide to the eye.

proportionally enhanced stability against creaming. However, as shown in Fig. 5 we observe that the 2 wt%  $\alpha$ -ZrP-TBA (and 1 wt% Span 80) destabilizes within 1 day of preparation, whereas the 5 wt%  $\alpha$ -ZrP-TBA (and 1 wt% Span 80) is stable for at least 1 month, which is much more than the 2.5x factor based on enhanced viscosity. Therefore, the enhanced viscosity of the high concentration nanosheet dispersion is not responsible for the long-term stability.

### 3.4. Droplet morphology and aggregation in emulsions stabilized by combination emulsifiers

Emulsion stability is determined by the size, shape, and aggregation state of droplets. We, therefore, used optical microscopy to qualitatively examine the droplet morphology and extent of aggregation in emulsions stabilized by the combination emulsifiers with Span 80 being fixed at 1 wt% and varying amounts of  $\alpha$ -ZrP-TBA nanosheets (Fig. 6). The microscopy images were taken just after the preparation of the emulsion.

In the absence of a nanosheet (i.e., in the Span 80 alone system), the droplets are spherical for both W/O and O/W emulsions, as shown in Fig. 6a. The W/O droplets appear aggregated, and larger O/W emulsion droplets were observed after the inversion point,  $\phi_w > 0.3$ . However, the oil droplets become smaller at a high volume fraction of water. After adding the  $\alpha$ -ZrP-TBA nanosheets, in the W/O emulsions, small droplets are formed with less aggregation compared to the Span 80 alone system, as shown in (Fig. 6(b(1–3))–(e(1–3))).

A striking finding is that we observe nonspherical or elongated oil droplets after the phase inversion point (Fig. 6(b(5–7))–(e(5–7))) when combination emulsifiers are used, and not when just the Span 80 or the nanosheet is used during emulsification. Thus, the addition of nanosheet appears to facilitate the formation of rod-shaped oil droplets. This

nonspherical droplet morphology is most prominent in the O/W emulsions with less oil content (i.e.  $\phi_w = 0.8, 0.9$ ). With increasing nanosheet concentration, the nonspherical character of droplets was enhanced, and less aggregation was observed.

The above observations on the microstructure of the emulsion inform on emulsion stability observed for O/W emulsions at high nanosheet loading. It appears that the less aggregation and nonspherical character inhibit creaming in the O/W emulsions at high water fraction, promoting stability over a period of month. We also checked whether the rod-shaped droplets persist over long-term storage and found that non-sphericity is still present even after a month of storage.

### 3.5. Nanosheet and Span 80 interact synergistically to promote non-sphericity in emulsion droplets

Next, we considered the role that Span 80 plays in promoting nonspherical droplets in O/W emulsions. We varied the Span 80 concentration (0.1, 0.5, 1.0 wt%) and fixed the nanosheet concentration at 5 wt%. From the optical micrographs, it was observed that the droplet size decrease with increasing Span 80 concentration (Fig. 7a). The non-sphericity of oil droplets increases with increasing Span 80 concentration. We measured the aspect ratio (AR) of the droplets with  $AR \approx 1$  indicating spherical droplets and  $AR > 1$  indicating rod-shaped droplets. At 0.1, 0.5 and 1 wt% Span 80 concentrations, we observe AR values predominantly lie in the range of 1–1.5, 2–3.5, 2.5–6 respectively. Thus, increasing Span 80 concentration increases the elongational character of the droplets formed by using the combination emulsifier system.

Our results thus far show that increasing both the nanosheet concentration and the Span 80 concentration promotes the non-sphericity of the droplets indicating that they interact synergistically at the interface

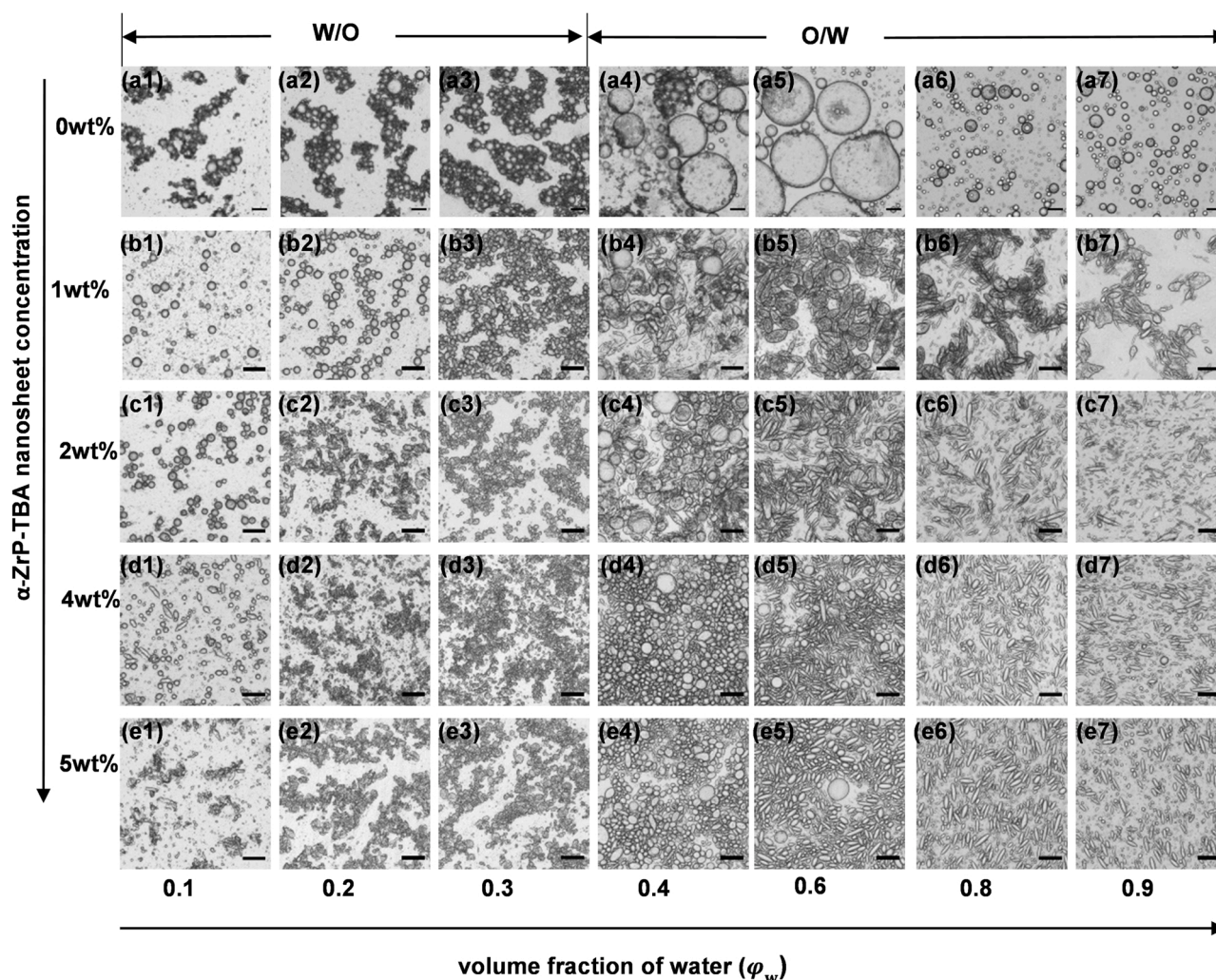


**Fig. 6.** Effect of  $\alpha$ -ZrP-TBA nanosheets concentration on droplet morphology. Optical micrographs of emulsion stabilized by combination of  $\alpha$ -ZrP-TBA nanosheet and Span 80 at different nanosheet concentrations, which were taken immediately after preparation. The volume fraction of water is indicated below the figure. The concentration of the  $\alpha$ -ZrP-TBA nanosheet is indicated on the left side of the figure. The Span 80 concentration (1 wt%) in mineral oil is fixed for all systems. The scale bar is 50  $\mu\text{m}$ . evaluated upto 3 months after preparation. Lines are a guide to the eye.

to potentially create jammed interfaces that are difficult to relax once the emulsions are made. To verify that the formation of the rod-shaped droplets is not sensitive to the details of our vortex-based emulsification technique, we also tested simple hand-shaking based technique. From Fig. 8, it is observed that both vortex mixing (Fig. 8a) and hand-shaking (Fig. 8b) emulsification produce non-spherical droplets of similar shape, i.e. we only observed rod-shaped droplets, and no other types of non-spherical droplets. With longer mixing times, we observe smaller elongated droplets in both cases. Additionally, the hand-shaking appears to produce larger non-spherical droplets than vortex-based mixing probably due to lower energy input. These results suggest that the interaction between nanosheet and Span 80 to promote non-spherical droplets is not sensitive to the details of the emulsification procedure. Furthermore, they highlight the simplicity, robustness, and scalability of our combination emulsifier approach to produce rod-shaped O/W emulsions.

### 3.6. Mechanism of formation of non-spherical droplets

An important finding from our combination emulsifier system is the production of anisotropic shaped droplets, particularly at high water fraction and nanosheet loading. Prior studies that have used 2D nanomaterials as emulsifiers in addition to surfactants did not report such a finding (see Table 1). The emulsion stabilized by surfactant alone forms

a spherical shape in the absence of external force since the fluid-like interface can relax to minimize surface energy [1]. Emulsion droplets of nonspherical geometry have been observed in Pickering emulsions, where exposing droplets to external fields, stretches the interface and induces jamming to form a solid-like interface that prevents relaxation to spherical shape [62]. In our case since we do not observe nonspherical droplets when emulsions are made with a single emulsifier (Span 80 or  $\alpha$ -ZrP-TBA nanosheets) indicating that the adsorbed surfactant and nanosheet work together to create stable elongated droplets.

Our proposed mechanism is shown in Fig. 9. During bulk emulsification, due to elongational stresses, the coarse droplets deform and undergo breakup. Span 80 has higher diffusivity ( $3.96 \times 10^{-12} \text{ m}^2/\text{s}$ ) compared to the nanosheet ( $2.18 \times 10^{-13} \text{ m}^2/\text{s}$ ) due to its small size. As a result, we hypothesize that Span 80 adsorbs at the interface reducing the interfacial energy that allows more nanosheets to adsorb and jam the interface creating non-spherical droplets. Consistent with this hypothesis, we observe that both increasing Span 80 and nanosheet concentration promotes nonsphericity. Interestingly, we also observe tiny spherical droplets of diameter  $< 10 \mu\text{m}$  in these emulsions (Fig. 8), suggesting that strong interfacial jamming is not occurring at these length-scales to overcome the Laplace pressure. Thus, our combination emulsifier system produces non-sphericity in droplets beyond length scales of approximately  $10 \mu\text{m}$ .

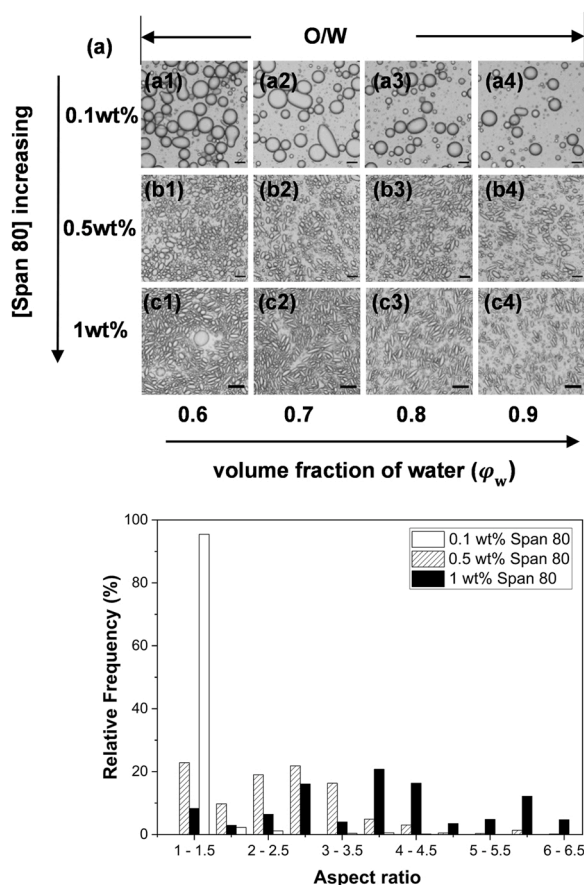


**Fig. 7.** Effect of surfactant concentration on the droplet morphology when emulsions are stabilized by the combination system of Span 80 and  $\alpha$ -ZrP-TBA nanosheets. (a) Optical micrographs of emulsion stabilized by 5 wt%  $\alpha$ -ZrP-TBA nanosheet and varying amounts of Span 80. Images were taken immediately after preparation. The volume fraction of water is indicated below the figure. The concentration of Span 80 is indicated on the left side of the figure. The scale bar is 50  $\mu\text{m}$ . (b) Aspect ratio of O/W emulsion droplets ( $\phi_w=0.9$ ) at different Span 80 concentrations and at a fixed  $\alpha$ -ZrP-TBA nanosheet concentration of 5 wt%.

An important premise underlying our proposed mechanism is that the interfacial properties resulting from the combination emulsifier system are rather different than those from Span 80 or nanosheet alone. To investigate the nature of interface resulting from these emulsifiers, we performed capillary breakup experiments as shown in Fig. 10. A co-flow capillary microfluidic device [58], was used to generate oil droplets in water (Fig. 10a), similar to our stable bulk emulsions. Four emulsifier conditions were tested that included (i) no-emulsifier (ii) 1 wt% Span 80 (iii) 5 wt%  $\alpha$ -ZrP-TBA nanosheet, and (iv) the combination emulsifier 5 wt%  $\alpha$ -ZrP-TBA nanosheet and 1 wt% Span 80. Neck thinning kinetics was obtained at the same dispersed phase and continuous phase flow rates for the four emulsifier conditions. In contrast to bulk emulsification, we note that the formed droplets in the co-flow device do not exhibit nonspherical shape probably due to weak elongational stresses or differences in kinetics of emulsifier adsorption.

Fig. 10b shows the images during the final stages of neck thinning and pinch-off. In Fig. 10c, we quantify the minimum neck diameter as a function of time. We observe that the neck diameter decreases very fast in the absence of emulsifiers. Both Span 80 or  $\alpha$ -ZrP-TBA nanosheet systems slow down the neck thinning in a similar fashion compared to the no-emulsifier case. Most strikingly, the combination emulsifier case shows that the neck thinning is significantly delayed, with the formation of thin cylindrical filaments that persists for much longer period than the single-emulsifier cases. This persistence of thin filament during capillary

pinch-off is a signature of a viscoelastic interface [63,64] that could be resulting from the solid-like interface promoted by nano-sheet jamming in the presence of Span 80.

In summary, these neck thinning results provide support to our proposed mechanism that interfacial resistance is strengthened by the combined effect of nanosheet and Span 80, probably due to enhanced adsorption of nanosheet mediated by Span 80.

## 4. Discussion

### 4.1. A combination emulsifier system that provides long-term emulsion stability

Layered 2D nanomaterials offer the potential to be used as particulate emulsifiers to stabilize emulsions. Among these the  $\alpha$ -ZrP-TBA nanosheets are unique as they are as easy to synthesize, aggregation-free in solution and the sheet geometry can be modified. Studies have previously used chemically modified nanosheets made from  $\alpha$ -ZrP particles to stabilize emulsions [48], but no studies have explored the role of combination emulsifiers where the  $\alpha$ -ZrP-TBA nanosheets were present in the aqueous phase and a lipophilic surfactant was present in the oil phase.

We found that the nanosheet or surfactant itself does not stabilize the emulsion. However, the inclusion of both the emulsifiers resulted in stable O/W emulsions for up to 3 months. Thus, there is a synergistic mechanism by which nanosheet and surfactant have ensured long-term stability against creaming. The emulsification process involves simultaneous events of droplet rupturing and re-coalescence [65]. Initially, there are available naked interfaces for emulsifier adsorption during emulsification. As surfactants are smaller in size ( $\sim 2$ – $3$  nm) compared to the size of nanosheets ( $\sim 1$   $\mu\text{m}$ ), their higher diffusivity might cover the newly formed interface resulting in delayed re-coalescence phenomena. This will further increase droplet breakup and produce smaller droplets. The reduced interfacial tension due to surfactant adsorption may allow the  $\alpha$ -ZrP-TBA nanosheets to assemble at the oil/water interface and ensure enough particle coverage providing long-term stability.

The adsorption rates of the surfactant and the nanosheets are expected to be dependent on their concentration which is consistent with our observations that the emulsion stability was found to be dependent on the concentrations of both Span 80 and  $\alpha$ -ZrP-TBA nanosheets, similar to some literature on mixed systems [26]. The droplet size was also affected by both the nanosheet and the surfactant concentration. The increase in surfactant concentration may promote the droplet breakup phenomena due to a more rapid reduction in interfacial tension and may also reduce re-coalescence events due to more efficient surface coverage. The higher concentration of nanosheets may also reduce re-coalescence events producing smaller droplets and stabilizing them.

### 4.2. Phase inversion occurs at a critical volume fraction

In our experiments, we found that at low water fractions, W/O emulsions are formed, and at high water fractions, O/W emulsions are produced. Phase inversion was found to occur at a critical water fraction  $\phi_{cw} = 0.3$  and was independent of the hydrophilic nanosheet and the lipophilic surfactant concentration. According to the Ostwald [66] model, the phase inversion occurs when the internal phase volume fraction ( $\phi_w$ ) of an emulsion reaches the close-packing volume fraction of hard spheres, i.e.,  $\phi_{cw} = 0.7$ . It is clear that the Ostwald model does not support our observations. Vaessen et al. explained that the catastrophic phase inversion is better understood with a kinetic approach based on droplet breakup and coalescence [67]. According to this model, the droplet size diverged above a critical volume fraction of 26.4%, indicating phase inversion without considering growth in the effective volume fraction of the dispersed phase. This meant that all droplets coalesced long before reaching the close packing point.

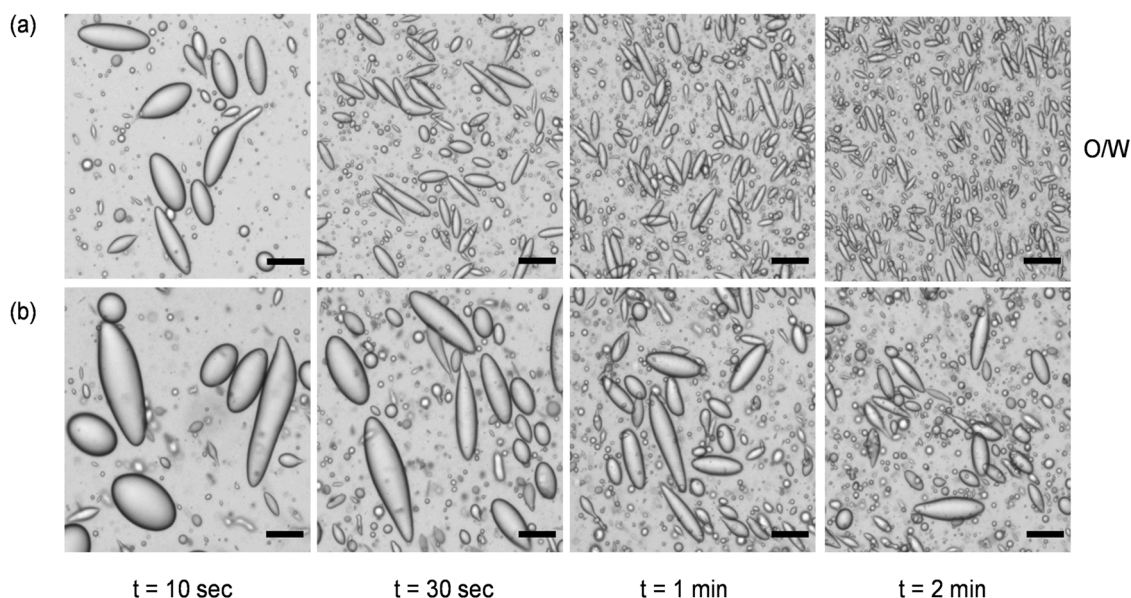


**Fig. 8.** Effect of emulsification method on non-sphericity of droplets. Optical micrographs of emulsion stabilized by combination of 5 wt%  $\alpha$ -ZrP-TBA nanosheet in water and 1 wt% Span 80 in mineral oil. Two different emulsification methods (a) vortex mixer @2000 rpm and (b) hand-shaking were used while mixing for different times. The images were taken immediately after preparation. The oil-in-water emulsion (O/W) is formed at volume fraction of water  $\phi_w = 0.9$ . The scale bar is 50  $\mu\text{m}$ .

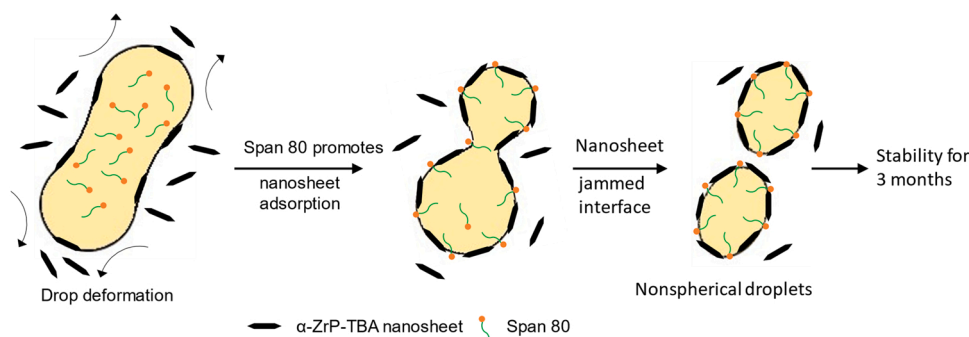


**Fig. 9.** Schematic of the mechanism of formation of nonspherical droplets in the presence of  $\alpha$ -ZrP-TBA nanosheet and Span 80.

In other experimental systems, studies show that the phase inversion volume fraction depends on the HLB value of the surfactant [68,69] and dispersed phase viscosity [70], stirring intensity [71]. For example, Galindo-Alvarez et al., [70] showed that for  $\text{HLB} > 10$ , phase inversion occurs at  $\phi_{cw} = 0.06$  or  $\phi_{cw} = 0.125$  depending on whether the dispersed phase viscosity was 12.5 Pa.s, or 1 Pa.s respectively. Likewise, when the HLB value  $< 10$ , the emulsions are W/O, with  $\phi_{cw} = 0.25$ –0.35 depending on the viscosity. Mira et al. [71] also showed that at  $\text{HLB} < 10$ , increasing the stirring speed from 600 rpm to 1500 rpm shifted the inversion point to the low volume fraction of water, resulting in  $\phi_{cw} = 0.19$ –0.35. A further increase in stirring speed from 1500 rpm to 6000 rpm could reduce the inversion point. In the case of  $\text{HLB} > 10$ , the increase in the stirring energy shifted the dynamic inversion line toward a higher volume fraction ( $\phi_{cw} = 0.7$ –0.9). Just like in surfactants, Binks et al. [72] investigated the phase inversion in Pickering emulsions using hydrophilic and hydrophobic silica particles. The phase inversion point for hydrophobic silica occurred at  $\phi_{cw} = 0.7$ , whereas for hydrophilic silica, the point was  $\phi_{cw} = 0.3$ .

In our case, for the Span 80 alone system (which has  $\text{HLB} = 4.3$  [73]), we also observed W/O emulsions form with phase inversion occurring at  $\phi_{cw} = 0.3$ , which is similar to that found by Galindo-Alvarez et al. [70] and Mira et al. [71]. With the  $\alpha$ -ZrP-TBA nanosheets, which are hydrophilic, we also found  $\phi_{cw} = 0.3$ , similar to hydrophilic silica. With

the combination emulsifier system, we observe phase inversion also occurring at  $\phi_{cw} = 0.3$ .

#### 4.3. Bulk-scale production of stable non-spherical droplets

Emulsions under quiescent conditions typically contain spherical droplets due to their interfacial energy. The ability to produce emulsions containing anisotropic shaped droplets might lead to novel functional properties including enhanced stability, unique rheology and drug delivery performance. Prior works to generate non-spherical droplets involved application of electrical or magnetic fields to deform droplet interface that promotes adsorption of nanoparticle surfactants to the interface [50–52]. The jammed particle-laden interfaces resist relaxation to spherical shape enabling production of non-spherical droplets. Although, elegant, these methods are inherently low throughput, motivating the need for alternative methods.

In this work, we show that the combination of nanosheet and Span 80 leads to the formation of elongated droplets, with an aspect ratio that is tunable by altering the concentrations of both these emulsifiers. We observe production of non-spherical droplets of size typically 10  $\mu\text{m}$  or larger with these droplets retaining their shape at least for a month. This contrasts with prior works, where non-spherical droplets of  $\sim 1$  mm were made [50,52], and moreover information on their long-term

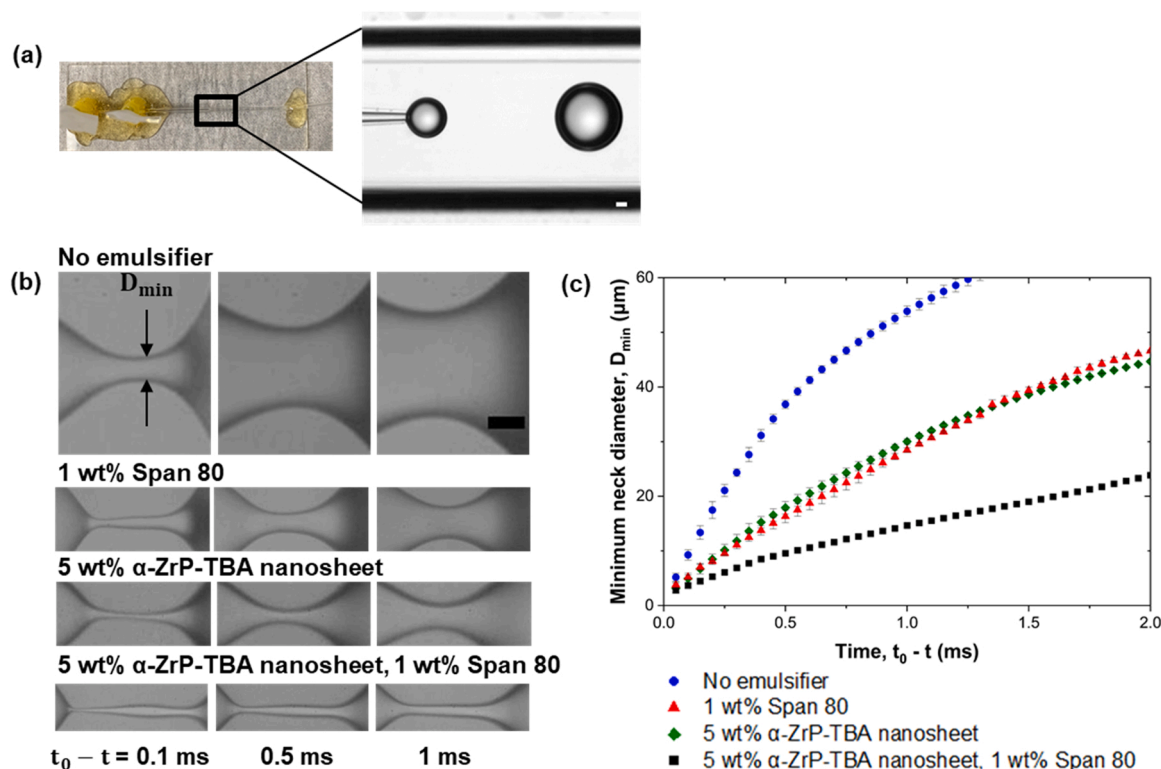


**Fig. 10.** Neck pinch-off kinetics in the dripping regime. (a) Hydrophilic co-flow geometry in glass-based capillary. (b) Time-stamped images of droplet breakup for no-emulsifier, Span 80,  $\alpha$ -ZrP-TBA nanosheet and combination of  $\alpha$ -ZrP-TBA nanosheet and Span 80. (c) Minimum neck diameter ( $D_{min}$ ) as a function of time where  $t$  is the time before the pinch-off at which the images were taken and  $t_0$  is the pinch-off time of the neck. Span 80 is in mineral oil which is a dispersed phase and  $\alpha$ -ZrP-TBA nanosheet in water phase as continuous phase. Dispersed phase flow rate  $Q_{in} = 0.5$  mL/h; Continuous phase flow rate  $Q_{out} = 80$  mL/h for all systems. The scale bar is  $30 \mu\text{m}$ .

stability is lacking. Importantly, these non-spherical droplets can be made using bulk emulsification that is insensitive to the precise details of the flow during emulsion production.

We find that the degree of droplet aspect ratio depends on both the Span 80 and nanosheet concentration and therefore the anisotropic shape is tunable to some extent. The mechanism underlying the non-spherical shape appears to be increased interfacial resistance offered by the a jammed particle interface. The capillary breakup experiments indicate a significantly delayed neck thinning in the presence of Span 80 and nanosheet, supporting the hypothesis of enhanced interfacial resistance.

## 5. Conclusions

A systematic investigation of emulsion type, stability and droplet morphology has been performed using Span 80,  $\alpha$ -ZrP-TBA nanosheets and their combination. The emulsion type was determined as a function of the volume fraction of water and nanosheet concentration. The catastrophic phase inversion was observed at  $\phi_{cw} = 0.3$  for all systems and is independent of nanosheet concentration.

The stability of emulsions against phase separation was investigated as a function of nanosheet and Span 80 concentration for 24 h and upto 3 months. The emulsions creamed within 24 h when only Span 80 or nanosheet was used as the emulsifier. However, when the combination emulsifier system was used the O/W emulsions were resistant to creaming for upto 3 months. Increasing the  $\alpha$ -ZrP-TBA nanosheet and Span 80 concentration made the O/W emulsions resistant to creaming suggesting that the combination emulsifier system promotes long-term emulsion stability.

Intriguingly, the morphology of the O/W emulsion droplets was found to be rod-shaped. Increasing the nanosheet and Span 80

concentrations increased the aspect ratio of the droplets suggesting that the emulsifier concentration could be used to tune the shape anisotropy. The morphology of O/W emulsion droplets further explains the synergistic effect. More nonspherical droplets are observed with increasing nanosheet concentration, indicating the nanosheet adsorption at the water-oil interface. The effect of Span 80 concentration on the nonspherical geometry of droplets was also studied and found that nonsphericity is enhanced by increasing the Span 80 concentrations. The synergistic effect of  $\alpha$ -ZrP-TBA nanosheet and Span 80 improved the emulsion stability, which was not possible to achieve with only the nanosheet or Span 80 as emulsifiers. The findings from this study suggest that a combination emulsifier approach that involves surfactants and particulate emulsifier in different phases could be a novel means to achieve long-term stability of emulsions.

## CRediT authorship contribution statement

**Nishat Anjum:** Investigation, Experiments, Data curation, Writing – original draft, Writing – review & editing. **Ya-Wen Chang:** Conceptualization, Investigation, Writing – original draft, Supervision. **Siva A. Vanapalli:** Conceptualization, Investigation, Writing – original draft, Writing – review & editing, Supervision.

## Declaration of Competing Interest

The authors declare that they have no known competing financial interests or personal relationships that could have appeared to influence the work reported in this paper.

## Acknowledgements

Acknowledgment is made to the Donors of the American Chemical Society Petroleum Research Fund for support of this research. We are grateful to Masoud Norouzi Darabad for developing the image processing code for determining neck thinning during drop breakup.

## References

- [1] B. Binks, *Modern Aspects of Emulsion Science*, Royal Soc. Chem, Cambridge, 1998.
- [2] B.P. Binks, Particles as surfactants—similarities and differences, *Curr. Opin. Colloid Interface Sci.* 7 (1) (2002) 21–41.
- [3] S.U. Pickering, Cxvi.—emulsions, *J. Chem. Soc., Trans.* 91 (1907) 2001–2021.
- [4] R. Aveyard, B.P. Binks, J.H. Clint, Emulsions stabilised solely by colloidal particles, *Adv. Colloid Interface Sci.* 100–102 (2003) 503–546.
- [5] S. Fujii, E.S. Read, B.P. Binks, S.P. Armes, Stimulus-responsive emulsifiers based on nanocomposite microgel particles, *Adv. Mater.* 17 (8) (2005) 1014–1018.
- [6] N. Saleh, T. Sarbu, K. Sirk, G.V. Lowry, K. Matyjaszewski, R.D. Tilton, Oil-in-water emulsions stabilized by highly charged polyelectrolyte-grafted silica nanoparticles, *Langmuir* 21 (22) (2005) 9873–9878.
- [7] B.R. Midmore, Synergy between silica and polyoxyethylene surfactants in the formation of O/W emulsions, *Colloids Surf. A Physicochem. Eng. Asp.* 145 (1) (1998) 133–143.
- [8] B.P. Binks, A. Desforges, D.G. Duff, Synergistic stabilization of emulsions by a mixture of surface-active nanoparticles and surfactant, *Langmuir* 23 (3) (2007) 1098–1106.
- [9] B.P. Binks, J.A. Rodrigues, Enhanced stabilization of emulsions due to surfactant-induced nanoparticle flocculation, *Langmuir* 23 (14) (2007) 7436–7439.
- [10] B.P. Binks, J.A. Rodrigues, W.J. Frith, Synergistic interaction in emulsions stabilized by a mixture of silica nanoparticles and cationic surfactant, *Langmuir* 23 (7) (2007) 3626–3636.
- [11] C.P. Whitby, D. Fornasiero, J. Ralston, Effect of adding anionic surfactant on the stability of Pickering emulsions, *J. Colloid Interface Sci.* 329 (1) (2009) 173–181.
- [12] G.R. Gray, H.C. Darley, W.F. Rogers, *Composition and Properties of Oil Well Drilling Fluids*, Gulf Publishing Company, Book Division, 1980.
- [13] L.N. Butler, C.M. Fellows, R.G. Gilbert, Effect of surfactants used for binder synthesis on the properties of latex paints, *Prog. Org. Coat.* 53 (2) (2005) 112–118.
- [14] N.G. Eskandar, S. Simovic, C.A. Prestidge, Synergistic effect of silica nanoparticles and charged surfactants in the formation and stability of submicron oil-in-water emulsions, *Phys. Chem. Chem. Phys.* 9 (48) (2007) 6426–6434.
- [15] B.P. Binks, J.A. Rodrigues, Double inversion of emulsions by using nanoparticles and a di-chain surfactant, *Angew. Chem.* 119 (28) (2007) 5485–5488.
- [16] L. Torres, R. Iturbe, M. Snowden, B. Chowdhry, S. Leharne, Preparation of o/w emulsions stabilized by solid particles and their characterization by oscillatory rheology, *Colloids Surf. A Physicochem. Eng. Asp.* 302 (1–3) (2007) 439–448.
- [17] Z.-G. Cui, K.-Z. Shi, Y.-Z. Cui, B. Binks, Double phase inversion of emulsions stabilized by a mixture of CaCO<sub>3</sub> nanoparticles and sodium dodecyl sulphate, *Colloids Surf. A Physicochem. Eng. Asp.* 329 (1–2) (2008) 67–74.
- [18] J. Wang, F. Yang, C. Li, S. Liu, D. Sun, Double phase inversion of emulsions containing layered double hydroxide particles induced by adsorption of sodium dodecyl sulfate, *Langmuir* 24 (18) (2008) 10054–10061.
- [19] J. Wang, G. Liu, L. Wang, C. Li, J. Xu, D. Sun, Synergistic stabilization of emulsions by poly (oxypropylene) diamine and Laponite particles, *Colloids Surf. A Physicochem. Eng. Asp.* 353 (2–3) (2010) 117–124.
- [20] J. Dong, A.J. Worthen, L.M. Foster, Y. Chen, K.A. Cornell, S.L. Bryant, T. M. Truskett, C.W. Bielawski, K.P. Johnston, Modified montmorillonite clay microparticles for stable oil-in-seawater emulsions, *ACS Appl. Mater. Interfaces* 6 (14) (2014) 11502–11513.
- [21] J. Zhang, L. Li, J. Xu, D. Sun, Effect of cetyltrimethylammonium bromide addition on the emulsions stabilized by montmorillonite, *Colloid Polym. Sci.* 292 (2) (2014) 441–447.
- [22] J.H. Schulman, J. Leja, Control of contact angles at the oil-water-solid interfaces. Emulsions stabilized by solid particles (BaSO<sub>4</sub>), *Trans. Faraday Soc.* 50 (1954) 598–605.
- [23] D.E. Tambe, M.M. Sharma, Factors controlling the stability of colloid-stabilized emulsions: I. An experimental investigation, *J. Colloid Interface Sci.* 157 (1) (1993) 244–253.
- [24] G. Lagaly, M. Reese, S. Abend, Smectites as colloidal stabilizers of emulsions: I. Preparation and properties of emulsions with smectites and nonionic surfactants, *Appl. Clay Sci.* 14 (1) (1999) 83–103.
- [25] C.P. Whitby, D. Fornasiero, J. Ralston, Effect of oil soluble surfactant in emulsions stabilised by clay particles, *J. Colloid Interface Sci.* 323 (2) (2008) 410–419.
- [26] R. Pichot, F. Spyropoulos, I. Norton, Mixed-emulsifier stabilised emulsions: Investigation of the effect of monoolein and hydrophilic silica particle mixtures on the stability against coalescence, *J. Colloid Interface Sci.* 329 (2) (2009) 284–291.
- [27] J. Wang, F. Yang, J. Tan, G. Liu, J. Xu, D. Sun, Pickering emulsions stabilized by a lipophilic surfactant and hydrophilic platelike particles, *Langmuir* 26 (8) (2010) 5397–5404.
- [28] J. Zhang, L. Li, J. Wang, J. Xu, D. Sun, Phase inversion of emulsions containing a lipophilic surfactant induced by clay concentration, *Langmuir* 29 (12) (2013) 3889–3894.
- [29] T. Nallamilli, M.G. Basavaraj, Synergistic stabilization of Pickering emulsions by in situ modification of kaolinite with non ionic surfactant, *Appl. Clay Sci.* 148 (2017) 68–76.
- [30] B.P. Binks, S.O. Lumsdon, Pickering emulsions stabilized by monodisperse latex particles: effects of particle size, *Langmuir* 17 (15) (2001) 4540–4547.
- [31] B. Madivala, S. Vandebriel, J. Franssaer, J. Vermant, Exploiting particle shape in solid stabilized emulsions, *Soft Matter* 5 (8) (2009) 1717–1727.
- [32] Y. Yang, Z. Liu, D. Wu, M. Wu, Y. Tian, Z. Niu, Y. Huang, Edge-modified amphiphilic Laponite nano-discs for stabilizing Pickering emulsions, *J. Colloid Interface Sci.* 410 (2013) 27–32.
- [33] W. Li, L. Yu, G. Liu, J. Tan, S. Liu, D. Sun, Oil-in-water emulsions stabilized by Laponite particles modified with short-chain aliphatic amines, *Colloids Surf. A Physicochem. Eng. Asp.* 400 (2012) 44–51.
- [34] N.P. Ashby, B.P. Binks, Pickering emulsions stabilised by Laponite clay particles, *Phys. Chem. Chem. Phys.* 2 (24) (2000) 5640–5646.
- [35] M.V. Tzoumaki, T. Moschakis, V. Kiosseoglou, C.G. Biliaderis, Oil-in-water emulsions stabilized by chitin nanocrystal particles, *Food Hydrocoll.* 25 (6) (2011) 1521–1529.
- [36] M. Shen, D.E. Resasco, Emulsions stabilized by carbon nanotube– silica nanohybrids, *Langmuir* 25 (18) (2009) 10843–10851.
- [37] H. Wang, E.K. Hobbie, Amphiphobic carbon nanotubes as macroemulsion surfactants, *Langmuir* 19 (8) (2003) 3091–3093.
- [38] H. Wu, W. Yi, Z. Chen, H. Wang, Q. Du, Janus graphene oxide nanosheets prepared via Pickering emulsion template, *Carbon* 93 (2015) 473–483.
- [39] K.Y. Yoon, S.J. An, Y. Chen, J.H. Lee, S.L. Bryant, R.S. Ruoff, C. Huh, K.P. Johnston, Graphene oxide nanoplatelet dispersions in concentrated NaCl and stabilization of oil/water emulsions, *J. Colloid Interface Sci.* 403 (2013) 1–6.
- [40] Y. He, F. Wu, X. Sun, R. Li, Y. Guo, C. Li, L. Zhang, F. Xing, W. Wang, J. Gao, Factors that affect pickering emulsions stabilized by graphene oxide, *ACS Appl. Mater. Interfaces* 5 (11) (2013) 4843–4855.
- [41] J. Kim, L.J. Cote, F. Kim, W. Yuan, K.R. Shull, J. Huang, Graphene oxide sheets at interfaces, *J. Am. Chem. Soc.* 132 (23) (2010) 8180–8186.
- [42] M.A. Creighton, Y. Ohata, J. Miyawaki, A. Bose, R.H. Hurt, Two-dimensional materials as emulsion stabilizers: interfacial thermodynamics and molecular barrier properties, *Langmuir* 30 (13) (2014) 3687–3696.
- [43] V. Nicolosi, M. Chhowalla, M.G. Kanatzidis, M.S. Strano, J.N. Coleman, Liquid exfoliation of layered materials, *Science* 340 (6139) (2013), 1226419.
- [44] M. Shuai, A.F. Mejia, Y.-W. Chang, Z. Cheng, Hydrothermal synthesis of layered  $\alpha$ -zirconium phosphate disks: control of aspect ratio and polydispersity for nano-architecture, *CrystEngComm* 15 (10) (2013) 1970–1977.
- [45] L. Sun, W.J. Boo, H.-J. Sue, A. Clearfield, Preparation of  $\alpha$ -zirconium phosphate nanoplatelets with wide variations in aspect ratios, *New J. Chem.* 31 (1) (2007) 39–43.
- [46] B. Dan, N. Behabtu, A. Martinez, J.S. Evans, D.V. Kosynkin, J.M. Tour, M. Pasquali, I.I. Smalyukh, Liquid crystals of aqueous, giant graphene oxide flakes, *Soft Matter* 7 (23) (2011) 11154–11159.
- [47] K.S. Novoselov, D. Jiang, F. Schedin, T. Booth, V. Khotkevich, S. Morozov, A. K. Geim, Two-dimensional atomic crystals, *Proc. Natl. Acad. Sci. USA* 102 (30) (2005) 10451–10453.
- [48] A.F. Mejia, A. Diaz, S. Pulella, Y.-W. Chang, M. Simonetty, C. Carpenter, J. D. Battaes, M.S. Mannan, A. Clearfield, Z. Cheng, Pickering emulsions stabilized by amphiphilic nano-sheets, *Soft Matter* 8 (40) (2012) 10245–10253.
- [49] J.S. Guevara, A.F. Mejia, M. Shuai, Y.-W. Chang, M.S. Mannan, Z. Cheng, Stabilization of Pickering foams by high-aspect-ratio nano-sheets, *Soft Matter* 9 (4) (2013) 1327–1336.
- [50] M. Cui, T. Emrick, T.P. Russell, Stabilizing liquid drops in nonequilibrium shapes by the interfacial jamming of nanoparticles, *Science* 342 (6157) (2013) 460–463.
- [51] C. Huang, Z. Sun, M. Cui, F. Liu, B.A. Helms, T.P. Russell, Structured liquids with pH-triggered reconfigurability, *Adv. Mater.* 28 (31) (2016) 6612–6618.
- [52] X. Liu, N. Kent, A. Ceballos, R. Streubel, Y. Jiang, Y. Chai, P.Y. Kim, J. Forth, F. Hellman, S. Shi, Reconfigurable ferromagnetic liquid droplets, *Science* 365 (6450) (2019) 264–267.
- [53] J. Kim, S.A. Vanapalli, Microfluidic production of spherical and nonspherical fat particles by thermal quenching of crystallizable oils, *Langmuir* 29 (39) (2013) 12307–12316.
- [54] M. Caggioni, A.V. Bayles, J. Lenis, E.M. Furst, P.T. Spicer, Interfacial stability and shape change of anisotropic endoskeleton droplets, *Soft Matter* 10 (38) (2014) 7647–7652.
- [55] T. s A. Prilesky, E.M. Furst, Fluid networks assembled from endoskeletal droplets, *Chem. Mater.* 28 (11) (2016) 3734–3740.
- [56] B.P. Binks, S.O. Lumsdon, Transitional phase inversion of solid-stabilized emulsions using particle mixtures, *Langmuir* 16 (8) (2000) 3748–3756.
- [57] V.R. Dugyala, J.S. Muthukuru, E. Mani, M.G. Basavaraj, Role of electrostatic interactions in the adsorption kinetics of nanoparticles at fluid–fluid interfaces, *Phys. Chem. Chem. Phys.* 18 (7) (2016) 5499–5508.
- [58] A. Utada, L.-Y. Chu, A. Fernandez-Nieves, D. Link, C. Holtze, D. Weitz, Dripping, jetting, drops, and wetting: The magic of microfluidics, *MRS Bull.* 32 (9) (2007) 702–708.
- [59] L. Zhang, W. Gorset, M.J. Dresser, K.M. Giacomini, The interaction of n-tetraalkylammonium compounds with a human organic cation transporter, hOCT1, *J. Pharmacol. Exp. Ther.* 288 (3) (1999) 1192–1198.
- [60] K. Tamaki, The surface activity of tetrabutylammonium halides in the aqueous solutions, *Bull. Chem. Soc. Jpn.* 40 (1) (1967) 38–41.
- [61] National Center for Biotechnology Information. "PubChem Compound Summary for CID 9920342, Sorbitan monooleate" PubChem, (<https://pubchem.ncbi.nlm.nih.gov/compound/Sorbitan-monooleate>). (Accessed 7 September, 2021). 2021.

- [62] W. Ramsden, Separation of solids in the surface-layers of solutions and 'suspensions' (observations on surface-membranes, bubbles, emulsions, and mechanical coagulation).—preliminary account, *Proc. R. Soc. Lond.* 72 (1903) 156–164.
- [63] S.L. Anna, G.H. McKinley, Elasto-capillary thinning and breakup of model elastic liquids, *J. Rheol.* 45 (1) (2001) 115–138.
- [64] C.X. Zhao, E. Miller, J.J. Cooper-White, A.P. Middelberg, Effects of fluid–fluid interfacial elasticity on droplet formation in microfluidic devices, *AIChE J.* 57 (7) (2011) 1669–1677.
- [65] T.F. Tadros, Emulsion science and technology: a general introduction, *Emuls. Sci. Technol.* 1 (2009) 1–55.
- [66] W. Ostwald, Beiträge zur Kenntnis der Emulsionen, *Z. Chem. Ind. Kolloide* 6 (2) (1910) 103–109.
- [67] G. Vaessen, M. Visschers, H. Stein, Predicting catastrophic phase inversion on the basis of droplet coalescence kinetics, *Langmuir* 12 (4) (1996) 875–882.
- [68] J. Salager, M. Minana-Perez, M. Perez-Sanchez, M. Ramfrez-Gouveia, C. Rojas, Surfactant-oil-water systems near the affinity inversion part iii: the two kinds of emulsion inversion, *J. Dispers. Sci. Technol.* 4 (3) (1983) 313–329.
- [69] J.L. Salager, Phase transformation and emulsion inversion on the basis of catastrophe theory, *Encycl. Emuls. Technol.* 3 (1988) 79–134.
- [70] J. Galindo-Alvarez, V. Sadtler, L. Choplin, J.-L. Salager, Viscous oil emulsification by catastrophic phase inversion: influence of oil viscosity and process conditions, *Ind. Eng. Chem. Res.* 50 (9) (2011) 5575–5583.
- [71] I. Mira, N. Zambrano, E. Tyrode, L. Márquez, A.A. Peña, A. Pizzino, J.-L. Salager, Emulsion catastrophic inversion from abnormal to normal morphology. 2. Effect of the stirring intensity on the dynamic inversion frontier, *Ind. Eng. Chem. Res.* 42 (1) (2003) 57–61.
- [72] B.P. Binks, S.O. Lumsdon, Catastrophic Phase Inversion of Water-in-Oil Emulsions Stabilized by Hydrophobic Silica, *Langmuir* 16 (6) (2000) 2539–2547.
- [73] Needs, A., *Time-saving Guide to Emulsifier Selection*, 1976.